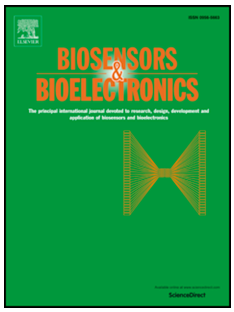

Sensitive and selective ctDNA detection based on functionalized black phosphorus nanosheets

Chi Huang, Shushu Hu, Xue Zhang, Haodong Cui, Lie Wu, Na Yang, Wenhua Zhou, Paul K. Chu, Xue-Feng Yu

PII: S0956-5663(20)30378-X

DOI: https://doi.org/10.1016/j.bios.2020.112384

Reference: BIOS 112384

To appear in: *Biosensors and Bioelectronics*

Received Date: 8 October 2019

Revised Date: 3 June 2020

Accepted Date: 9 June 2020

Please cite this article as: Huang, C., Hu, S., Zhang, X., Cui, H., Wu, L., Yang, N., Zhou, W., Chu, P.K., Yu, X.-F., Sensitive and selective ctDNA detection based on functionalized black phosphorus nanosheets, *Biosensors and Bioelectronics* (2020), doi: https://doi.org/10.1016/j.bios.2020.112384.

Chi Huang: Conceptualization, Methodology, Writing- Original draft preparation
Shushu Hu: Resources, Writing- Original draft preparation.
Xue Zhang: Formal analysis:
Haodong Cui: Resources
Lie Wu: Resources
Na Yang: Resources
Wenhua Zhou: Conceptualization, Reviewing and Editing, Investigation.
Paul K. Chu: Reviewing and Editing,
Xue-Feng Yu: Conceptualization, Reviewing and Editing,

Sensitive and selective ctDNA detection based on functionalized black phosphorus nanosheets

Chi Huang,[a,b] Shushu Hu,[a] Xue Zhang,[b] Haodong Cui,[b] Lie Wu,[b] Na Yang,[b] Wenhua Zhou,*[b] Paul K. Chu,[c] and Xue-Feng Yu*[b]

[a] *Chi Huang, Shushu Hu. Institute of Chemical Biology and Nanomedicine, Molecular Science and Biomedicine Laboratory, State Key Laboratory of Chemo/Biosensing and Chemometrics, College of Chemistry and Chemical Engineering, Hunan University, Changsha 410082, China*

[b] *Haodong Cui, Lie Wu, Wenhua Zhou, Xue-Feng Yu. Materials Interfaces Center, Shenzhen Institutes of Advanced Technology, Chinese Academy of Sciences, Shenzhen 518055, China*

[c] *Paul K. Chu Department of Physics and Department of Materials Science and Engineering, City University of Hong Kong, Tat Chee Avenue, Kowloon, Hong Kong, China*

ABSTRACT

Circulating tumor DNA (ctDNA) identification is one of the most meaningful approaches towards early cancer diagnosis. However, effective and practical methods for analyzing this emerging class of biomarkers are still lacking. In this work, a biosensor based on nitrophenyl functionalized black phosphorus nanosheets (NP-BPs) is fabricated for sensitive and selective detection of ctDNA. In this work, a nitrophenyl functionalized black phosphorus nanosheets (NP-BPs) biosensor is fabricated for sensitive and selective detection of ctDNA. Due to the successful nitrophenyl functionalization, the NP-BPs biosensor shows higher quenching efficiency and stronger affinity towards single-stranded DNA (ssDNA), as compared with double-stranded DNA (dsDNA). Therefore, the NP-BPs biosensor exhibits 5.4-fold fluorescence enhancement when dye-labelled ssDNA probe forms dsDNA in the presence of its specific ctDNA target. This biosensor exhibits a detection limit of 50 fM and a wide linear detection range of 50 fM-80 pM, provides reliable readout in a short time (15 minutes). Moreover, the NP-BPs-based biosensor could be applied to discriminate single nucleotide polymorphisms in clinical serum samples. It is envisioned that the NP-BPs-based sensing platform has great potentials in early cancer diagnosis and monitoring cancer progression.

Keywords: ctDNA; Black phosphorus; Surface functionalization; Nitrophenyl; two-dimensional materials; Biosensor

1. Introduction

Obstacles in cancer therapy include tumor heterogeneity, tumor evolution, and delayed diagnosis.(Burrell et al. 2013; Castellanos-Gomez 2015; Murtaza et al. 2013) Thus, early and accurate cancer diagnosis is crucial for timely and effective treatments to reduce morbidity and mortality in cancer patients.(Fu and Wang 2018; Hu et al. 2017) Circulating tumor DNA (ctDNA) is the DNA liberated from cancer cells into the body fluid, which can be found in the early stage of cancer.(Newman et al. 2014) However, despite the clinical virtues, sensitive and selective detection of ctDNA is still challenging, mainly due to the low blood abundance and high background of nucleic acid fragments from normal cells in real samples.(Schwarzenbach et al. 2011) Various platforms have been developed for ctDNA identification, for instance, next-generation sequencing, real-time polymerase chain reaction (RT-PCR), and digital PCR, but these platforms still have drawbacks such as the high cost, lengthy process, and complicated operations.(Das et al. 2015; Hu et al. 2018; Taly et al. 2013; Zhou et al. 2016)

As an effective solution in early cancer diagnosis, gene analysis, and detection of genetic disorders, DNA biosensors have attracted substantial attention. (Cao et al. 2018; Garcia-Olmo et al. 2010; Gupta et al. 2013; Karimi-Maleh et al. 2015; Yola et al. 2014) In these DNA biosensors, especially those based on nucleic acid hybridization, their performances could be further enhanced by tuning the π−π stacking e□ect and hydrophobic properties. (Huang et al. 2018; Lee et al. 2018) Although considerable achievements have been made in highly sensitive and low-cost DNA biosensors pertaining to the interaction of DNA and nanoparticle (Wang et al. 2018), most DNA biosensors can't be applied to detect ctDNA directly in serum samples. Therefore, new diagnostic platforms for ctDNA identification with the satisfactory sensitivity, selectivity, and simplicity are highly desirable.

As a fledgling member of two-dimensional (2D) nanomaterials, black phosphorus nanosheets (BPs) have drawn tremendous attentions in biosensing.(Yew et al. 2017; Zhou et al. 2018a) BPs possess large surface-to-volume ratio due to corrugated system comprising the armchair or zigzag structure which enable efficient adsorption of biomolecules.(Castellanos-Gomez 2015; Zhou et al. 2018b). Although miRNA detection of BPs biosensor has been developed, the detection limit could be further improved with surface functionalization.(Yew et al. 2017; Zhou et al. 2018a) Moreover, bare BPs are relatively unstable under ambient conditions further hindering their applications as biosensors.

Herein, a new biosensor based on nitrophenyl BPs (NP-BPs) for sensitive and selective detection of ctDNA is fabricated. As shown in scheme 1, after successful NP functionalization, in the absence of the target ctDNA, the FAM-labelled single-stranded DNA (ssDNA) probe (P) could be effectively adsorbed onto the

* Corresponding author. *Email address: xf.yu@siat.ac.cn (*Xue-Feng Yu*); wh.zhou@siat.ac.cn(*Wenhua Zhou*).*

surface of NP-BPs and quenched by NP-BPs. In the presence of its complementary target ctDNA, the probe quickly forms

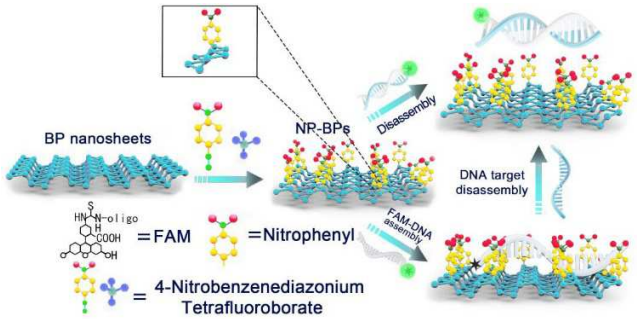

Scheme 1. Schematic design of NP-BPs-based biosensor for ctDNA detection based on the ssDNA/dsDNA discrimination ability. FAM is used as the fluorescence dye.

double stranded DNA (P/T) and couldn't adsorb on the surface of NP-BPs with fluorescence retained, which can be used to quantify the concentration of target ctDNA. This NP-BPs-based biosensor exhibiting high sensitivity, high selectivity, and short detection time has great potential pertaining to rapid and accurate detection of ctDNA.

2. Experimental section

2.1. Synthesis of NP-BPs.

The BPs were prepared by a liquid sonication exfoliation. 25 mg of the bulk BP was dispersed in 25 mL of NMP and treated ultrasonically for 10 hours. Bath sonication was carried out for another 10 hours at 300 W. Then 4-nitrophenyl-diazonium tetrafluoroborate (5 mg) was stirred with BPs (1 mg) in CH_3CN (1 mg BPs, 10 mL) for overnight to get NP-BPs. The prepared NP-BPs were rinsed with alcohol to terminate functionalization and remove unbonded 4-NPD molecules.

2.2. Concentration optimization of NP-BPs, $MgCl_2$, KCl.

To optimize the concentration of the NP-BPs, the FAM-labelled ssDNA (50 nM) was hybridized with the target DNA (50 nM) in 10 mM Tris-HCl buffer for 10 minutes. In the FL quenching assays, different volumes of the NP-BPs solution (100 μg/mL) of 0, 50, 75, 100, 125 and 150 μL were added to 10 mM Tris-HCl buffer (pH 7.4) for a total volume of 300 μL. The reaction proceeded for 15 minutes at room temperature and the fluorescence emission spectra were recorded at 520 nm. The concentrations of $MgCl_2$ and KCl were optimized with the same method.

2.3. Fluorescence quenching efficiency analysis.

Firstly, 50 nM of DNA probe was hybridized with 50 nM target ctDNA at room temperature for 10 minutes in bu ·er (10 mM Tris-HCl, 50 μM $MgCl_2$, and 50 mM KCl). The mixtures were then incubated with 10 μg/mL of NP-BPs for 15 minutes, and the fluorescence intensities were measured. The ssDNA probe quenching kinetics were recorded with the same procedure. For ssDNA, the quenching efficiency is defined as $(1-F_P/F_0) \times 100\%$, where F_P and F_0 are the FL intensities of dye-labelled ssDNA in the presence and absence of NP-BPs. For dsDNA, the quenching efficiency is defined as $(1-F_{P/T}/F_0) \times 100\%$, where $F_{P/T}$ and F_0 are the FL intensities of dsDNA in the presence and absence of NP-BPs, respectively.

2.4 Density functional theory calculations.

Periodic density functional theory calculations were carried out in the mixed Gaussian plane wave basis set as implemented in the CP2K code with Grimme's D3 dispersion corrections.(Grimme et al. 2010) The Perdew-Burke-Ernzerh generalized gradient approximation exchange correlation function (Perdew et al. 1996) was used to calculate the exchange correlation energy. The DZVP-MOLOPT basis set in combination with Geodecker-Teter-Hutter pseudopotentials (Goedecker et al. 1996) were used with a plane wave cutoff energy of 500 eV. The structural minimization was performed using Broyden–Fletcher–Goldfarb–Shanno algorithm.(William H. Press 2007) The BP (001) surface with the unit cell of 6x6 was built. Neighboring slabs were separated by a vacuum of 20 Å to avoid spurious self-interactions. Monkhorst-Pack k-point meshes of 5×5×1 were used for these periodic models.

2.5. Fluorescent ctDNA assays.

The clinical serum samples were collected by centrifugation at 3000 rpm for 10 minutes and frozen at -80 °C before usage. In the concentration gradient assays, the serum was spiked with 50 fM to 100 pM target ctDNA. Then ctDNA was extracted from 5 mL of serum using the MagMAX Cell-Free DNA Isolation Kit. Afterwards, the FAM-labelled ssDNA (50 nM) was hybridized with the extracted ctDNA for 10 minutes. Then, 10 μg/mL of NP-BPs were added to make a total volume of 300 μL and the fluorescence spectra were recorded. In the specificity assays, 0.5 pM of targets with different sequences were extracted from serum samples by following the same procedure, then the FAM-labelled ssDNA (50 nM) was hybridized for 10 minutes, and the fluorescence spectra were recorded.

2.6 *Quantitative PCR*

Pseudo-ctDNA targets were isolated with MagMAX Cell-Free DNA Isolation Kit from spiked serum according to the manufacturer's instruction. For a volume of 30 μL quantitative PCR (qPCR), 15 μL of 2 × reaction buffer, 1 μL Q5 enzyme (NEB), 10 μM primers and 1x SYBR Green I were used. Subsequent thermal cycling was performed at 98 °C for 0.5 minute, and then 45 cycles of 98°C for 10 seconds, 60 °C for 15 seconds and 72 °C for 10 seconds. Fluorescence signals were recorded with Bio-Rad PCR system (CFX96) after each cycle, and the threshold cycle (Ct) was calculated by the Bio-Rad analysis system. The oligonucleotide primers and target are shown in Table S1.

3. Results and discussion

3.1. Synthesis and characterizations of NP-BPs.

The BPs are exfoliated from bulk BP crystal by the liquid sonication exfoliation method.(Guo et al. 2015) An excess amount of 4-nitrophenyl diazonium tetrafluoroborate (4-NPD) is added to the BPs solution to allow NP-

functionalization.(Ryder et al. 2016) The bare BPs and NP-BPs are characterized by transmission electron microscopy (TEM), high-resolution TEM (HR-TEM), and atomic force microscopy (AFM). As shown in Fig. 1a and Fig. S1a, both bare BPs and

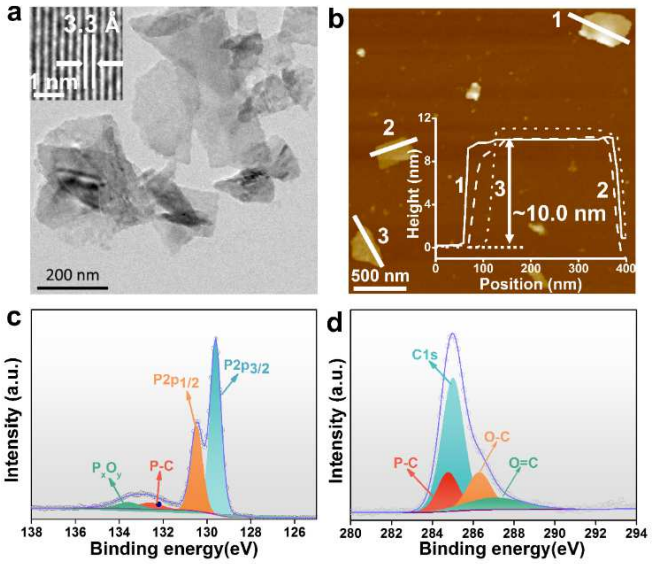

Fig. 1. Characterizations of NP-BPs. (a) TEM and inset HR-TEM images. (b) AFM image with height profiles along the white lines in the inset. (c) HR-XPS of P spectra. (d) HR-XPS of C spectra.

NP-BPs have average lateral sizes of ~300 nm. HR-TEM image reveals lattice fringes of 3.3 Å arising from (021) plane, indicating that lattice structure of BPs is preserved during NP-functionalization. The AFM images (Fig. 1b and S1b) confirm that the height increases from 8.7 nm of the bare BPs to 10.0 nm of the NP-BPs, confirming successful NP-functionalization. NP-functionalization of BPs is further corroborated by high-resolution X-ray photoelectron spectroscopy (HR-XPS) (Fig. 1c and 1d). In P-spectra, the NP-BPs exhibit dominant P peaks of P 2p2/3 and P 2p1/2 at 129.6 and 130.5 eV originating from P-P covalent bonds as well as a broad peak at 132.5 eV from P-C covalent bonds of phosphorus-phenyl compounds. Furthermore, the P-C covalent bond at 284.5 eV is observed from the C-spectra. Raman scattering is performed to investigate NP-functionalization (Fig. S2). Compared to the bare BPs, three typical Raman peaks of NP-BPs blue-shift with decreasing intensities. After NP-functionalization, contact angle is changed from 54.2 ± 1° to 64.5 ± 0.2°, which indicates the NP-BPs are more hydrophobic (Fig. S3). Zeta potentials of BPs have changed from −34.63 ± 0.75 mV to −22.63 ± 0.40 mV (Fig. S4a, Supporting Information) and the average hydrodynamic sizes change from ~310 nm to ~350 nm correspondingly(Fig. S4b, Supporting Information).

3.2. NP-BPs stability evaluation.

Since reliable detection signal is crucial for biosensor, the effect of NP-functionalization on the stability of BPs is investigated. The bare BPs and NP-BPs are at the same concentration of 28 ppm and optical photographs and absorption spectra are acquired at predetermined time points. As shown in Fig. 2a, the bare BPs solution becomes transparent in 72 hours. In contrast, NP-BPs solution is stable for 72 hours. Furthermore, the absorption intensities of the bare BPs decrease quickly and show 70% degradation after 3 days, whereas those of the NP-BPs exhibit negligible degradation under ambient conditions (Fig. 2b). These results further confirm successful

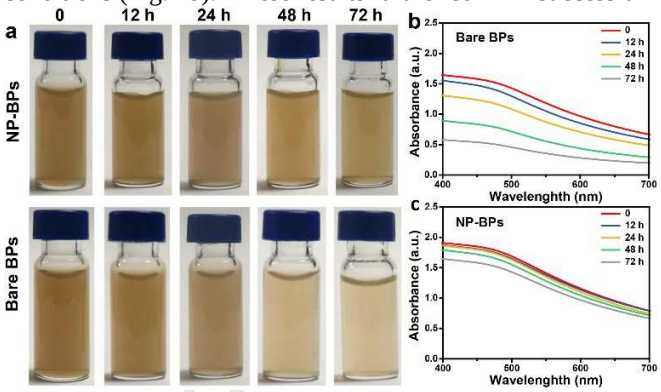

Fig. 2. Stability evaluation. (a) Optical photographs of NP-BPs and bare BPs dispersion in water. (b) Absorption spectrum of NP-BPs and (c) bare BPs under ambient after storing in water for 0, 12, 24, 48 and 72 h.

functionalization of BPs with NP, which protects the BPs from rapid degradation.

3.3. Optimization of the assay condition.

To optimize the biosensing performances of NP-BPs, the optimal concentration of NP-BPs in discriminating dsDNA and ssDNA is determined. As shown in Fig. S5a, the fluorescence intensities (FL intensity) from dye-labelled dsDNA are higher than that of dye-labelled ssDNA at the same NP-BPs concentration, thus providing preliminary evidence that the biosensor can discriminate ssDNA from dsDNA. Moreover, the FL intensities of the dsDNA and dye-labelled ssDNA change with increasing concentrations of NP-BPs. Fig. S5b shows the concentration-dependent fluorescence ratios of $F_{P/T}/F_P$ of NP-BPs. When the concentration of NP-BPs reaches 10.0 μg/mL, $F_{P/T}/F_P$ shows a value of 1.8 and further increase concentration of NP-BPs results in decreased $F_{P/T}/F_P$.

To verify the absorption performance, the NP-BPs and DNA are dispersed with various concentrations of $MgCl_2$ and KCl. The kinetics of fluorescence change are presented in Fig. S6 and Fig. S7. As shown in Fig. S6a and Fig. S7a, by increasing the concentrations of $MgCl_2$ or KCl, the absorption ability of NP-BPs towards ssDNA is strengthened. Since both of DNA and NP-BPs are negatively charged, repulsion effects between them may impede efficient absorption of DNA on NP-BPs. Cation ions, especially Mg^{2+} and K^+, has great affinity towards DNA. (Nikolay 1999) After adding cation ions, the negative charge of DNA are reduced, creating repulsion shielding effect between ssDNA and NP-BPs. On the other hand, because the negative charge density of dsDNA is higher than that of ssDNA, cation ions under certain concentration perform different repulsion shielding effects in these two species.(Shi et al. 2015) Thus, the optimized conditions are determined when ssDNA are fully shielded by cation ions and hence completely absorbed on the surface of NP-BPs, while only moderate shielding effect is observed in dsDNA (Fig. S6 and S7). The optimization

results are shown in Fig. S8 and Fig. S9. Hence, 10.0 μg/mL NP-BPs is used in the following experiments in concert with 50 μM Mg^{2+} and 50 μM K^{+}.

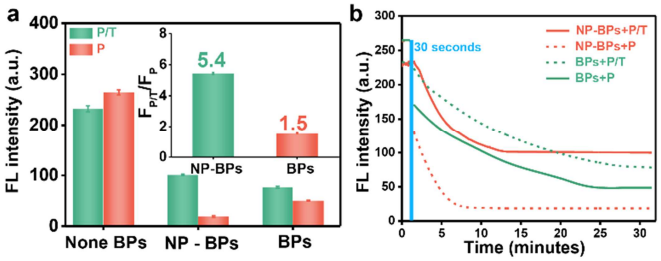

Fig. 3. Comparison of biosensing performance: (a) FL intensities of P/T (green histograms) and P (red histograms) in the presence of BPs, NP-BPs or none BPs. Inset: FL intensity ratios ($F_{P/T}/F_P$) in the presence of NP-BPs or BPs. The error bars represent the standard deviation of three samples under same condition. (b) Fluorescence quenching kinetics for P/T and P in the presence of NP-BPs or BPs (10 μg/mL) as a function of time. P represents the dye-labelled ssDNA and P/T represents dsDNA formed by the dye-labelled ssDNA and target DNA.

3.4. Fluorescence quenching property.

The interaction behavior between NP-BPs and single-stranded oligonucleotide probes with different lengths and fluorescent tags is determined. In this study, the lengths of FAM-labelled single-stranded oligonucleotide probes are set as 3-, 6-, 12-, 24-, 36- and 48-mer, respectively, and the concentration of all oligonucleotides is 50 nM. As shown in Fig. S10, the quenching efficiencies vary with different lengths of probes after adding NP-BPs (10.0 μg/mL). The lowest quenching efficiency is observed in the 3-mer oligonucleotide probe, mainly due to its weak interaction with NP-BPs, which is consistent with previous report.(Wang et al. 2013) With an increase in length of oligonucleotide, quenching efficiencies are elevated accordingly. However, when the length of the oligonucleotide probe is longer than 24-mer, the quenching efficiency shows a significant decrease, which possibly due to the departure of fluorescent tags from the surface of NP-BPs as previously reported.(Wang et al. 2013) The fluorescence quenching efficiency of NP-BPs is also investigated using ssDNA labelled with different fluorescent tags. As shown in Fig. S11, the NP-BPs-based biosensor exhibits high and similar quenching efficiencies toward all fluorescent tags tested. All these results indicate the fluorescence quenching is dominated by the adsorption of ssDNA to NP-BPs, rather than interaction between the fluorescent tags and NP-BPs.

3.5. Comparison biosensing performance of NP-BPs and BPs.

The discrimination ability towards dsDNA and ssDNA is investigated using NP-BPs and BPs. The concentrations of the dye-labelled ssDNA and target DNA are set as 50 nM and those of NP-BPs or bare BPs are 10.0 μg/mL. The FL intensities from dsDNA and dye-labelled ssDNA under different conditions are shown in Fig. 3a and the fluorescence emission spectra and fluorescence quenching efficiencies are presented in Fig. S12. In the absence of nanosheets, both dye-labelled ssDNA and dsDNA show strong FL intensities. After addition of NP-BPs, fluorescence from the dye-labelled ssDNA is nearly completely quenched with a quenching efficiency of 95.5% (Fig. S12b). However, when equal amount of target DNA is added to form dsDNA, FL quenching efficiency decreases to 55.3%. In contrast, for the bare BPs, the fluorescence quenching efficiency of the dye-labelled ssDNA is 81.5% and $F_{P/T}/F_P$ is only 1.5. These results demonstrate that NP-BPs biosensor has better performances in discriminating dsDNA and ssDNA than bare BPs. The outstanding performance of NP-BPs is also confirmed by fluorescence kinetics (Fig. 3b). The FL intensities are high and flat before adding NP-BPs. However, after adding NP-BPs, the FL intensity from the dye-labelled ssDNA (red dotted curve) quickly decreases and reach to a platform within 5 minutes and exhibits almost complete quenching after 8 minutes. On the other hand, in the presence of the target DNA, the FL intensity decreases slowly (red curve) after 10 minutes. In contrast, for the bare BPs, a much longer reaction time is required (25 minutes) for the quenching reaction to reach a plateau (green dotted and solid curves) and FL differences between dsDNA and ssDNA are much smaller as compared with NP-BPs. Therefore, besides increasing the overall stability of the biosensor, NP-functionalization improves the discrimination ability and response kinetics of the BPs biosensor.

Density functional theory calculations have been applied to ascertain the different affinity of NP-BPs towards ssDNA and dsDNA for NP-BPs. We select the Thymine from the DNA string as a model to calculate the Gibbs free energy. As shown in Fig. S13, the Gibbs free energy of interaction between NP-BPs and DNA nucleobase is much lower than that between NP-BPs and DNA phosphorous backbone. This difference mainly stems from the hydrophobic and π−π stacking interaction between DNA nucleobases and NP-BPs. Hydrophobic characteristic of nitrophenyl could enhance the interaction of NP-BPs and ssDNA because the hydrophobic groups of nucleotides. Moreover, like graphene, the aromatic structure of nitrophenyl could enhance the π−π stacking interaction between the nucleobases of ssDNA and aromatic structure on the surface of NP-BPs. However, the nucleobases are effectively shielded in the duplex after DNA hybridization, the hydrophobic interaction and π−π stacking interaction will be weakened and the dsDNA are thus desorbed from NP-BPs. (Zhang et al. 2015)

3.6. Sensitivity analysis.

The sensitivity of the NP-BPs biosensor pertaining to phosphoinositide 3-kinase catalytic subunit (PIK3CA) ctDNA is determined. PIK3CA gene plays an important role in activation of the downstream Alt signal transduction cascade, a pathway in the control of cell proliferation, migration, and survival.(Shukla et al. 2007) The hotspot mutation PIK3CA E542K G>A (rs121913273) resulting in the PI3KCA glutamate 542 to lysine mutation is selected as the target ctDNA (T1) because of its high-frequency mutation in breast, colorectal and gastric cancer.(Karakas et al. 2006; Kawano et al. 2006; Shukla et al. 2007) In the typical experiment, 50 nM dye-labeled ssDNA is hybridized with the ctDNA at concentrations between 0 and 100 nM. The mixture is incubated with NP-BPs for 15 minutes under the optimized conditions. As shown in

Fig. S14, S14, as the concentration of ctDNA increases, the FL intensity increases dramatically revealing a detection limit of 50 pM. The calibration curve between the FL intensity and

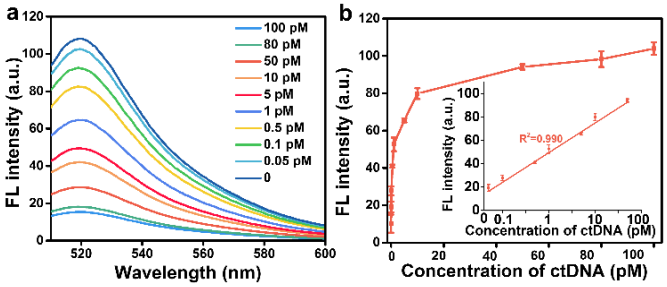

Fig. 4. Sensitivity of the NP-BPs-based biosensor in the detection of ctDNA: (a) Fluorescence emission spectrum (excited by 488 nm) in the presence of ctDNA (0, 0.05, 0.1, 0.5, 1, 5, 10, 50, 80, 100 pM). (b) Calibration curve of ctDNA detection in the buffer solution. Inset: Linear plot of the FL intensity versus concentration of ctDNA. The error bars represent the standard deviation of three samples under same condition.

concentration of ctDNA is derived (Fig. S14b) and a linear relationship between 50 pM and 50 nM (inset) is observed.

To assess the clinical potentials of the NP-BPs biosensor, it is applied to directly detect ctDNA in clinical serum samples. The clinical serum is kindly supplied by Shenzhen People's Hospital. The human serum samples are spiked with different concentrations of PIK3CA E542K G>A ctDNA. The concentrations of ssDNA probe and NP-BPs are 50 nM and 10 μg/mL in the serum samples, respectively. As shown in Fig. S15, the FL intensities increase gradually as the concentration of target ctDNA increases from 0 to 20 nM and a linear relationship between 0 to 5 nM is observed (Fig. S15b, inset). The detection limit of the NP-BPs biosensor is 0.5 nM in clinical serum, showing great application potential in real clinic serum samples. On the contrary, graphene oxide biosensor can't be applied directly in detecting ctDNA in serum samples, owing to the interference from strong nonspecific absorption of serum proteins (Table S2). (Hu et al. 2011) However, the performances of NP-BPs biosensor should be further improved for real applications.

In order to improve the detection limit in real application, the NP-BPs-based ctDNA biosensor is combined with the conventional magnetic extraction. The ctDNA is extracted from 5 mL of serum using the MagMAX Cell-Free DNA Isolation Kit. In the fluorescent assays, 50 nM dye-labelled ssDNA is hybridized with target ctDNA at concentrations between 0 and 100 pM. Then the mixture is incubated with NP-BPs for 15 minutes under the optimized conditions. As shown in Fig. 4a, the NP-BPs reveals a detection limit of 50 fM which is more sensitive compared with previously reported 2D nanosheet-based biosensors (Table S3). The calibration curve between the FL intensity and concentration of ctDNA is derived (Fig. 4b) and a linear relationship between 50 fM and 80 pM (inset) is observed, showing great application potential in the real clinic sample. Standard quantitative PCR is applied to confirm the actual concentration of the long target ctDNA. As shown in Fig. S16, the quantitative PCR results show a detection limit of 50 aM and a linear relationship of 50 aM-500fM. This linear relationship was subsequently used to validate the actual concentration of serially diluted ctDNA used in NP-BPs biosensor. Although NP-BPs biosensor is less sensitive as compared with the traditional quantitative PCR, this biosensor is comparatively simpler and faster, and thus has unique advantages in the point of care applications.

3.7. Robustness analysis.

Given the importance in distinguishing ssDNA and dsDNA, we further investigate whether NP-BPs biosensor is specific enough to discriminate single-stranded target ctDNA among di□erent dsDNA. dsDNA (50 nM) are formed through annealing before the addition of target ctDNA (50 nM). As shown in Fig. S17, when target ctDNA is mixed with dsDNA, the NP-BPs biosensor shows very low quenching efficiency. Moreover, when the dsDNA does not exist, the fluorescence quenching efficiency shows nearly the same value as compared with the mixture of ssDNA and dsDNA. These results demonstrate NP-BPs biosensor shows good discrimination ability towards ssDNA under the background interferences of dsDNA.

3.8. Specificity analysis.

The specificity of ctDNA detection poses a great challenge in early cancer diagnosis, prevention, and targeted therapy.(Huang et al. 2018) Inspired by the satisfactory performances of NP-BPs biosensor, its specificity in ctDNA detection is verified in both buffer and serum samples. Besides the target PIK3CA E542K G>A (T1, fully complementary to the probe), a series of single-base mismatch targets including PIK3CA E542K G>C (T2), PIK3CA E542K G>T (T3), and wild type (T4) have been designed. Other single-base mismatch targets including T6, T7, T8 and T9, single-nucleotide-deletion of PIK3CA E542K (T5) and short targets (T10, T11 and T12) are designed to evaluate the specificity of NP-BPs-based biosensor. As expected, the FL intensity of the target PIK3CA E542K G>A is approximately 5.7 times higher than those of other targets bearing single-base mismatches (Fig. 5b). Furthermore, our NP-BPs-based biosensor shows great specificity in the clinical serum sample with 0.5 nM ctDNA target (Fig. S18). These results demonstrate that the specificity of NP-BPs-based biosensor is sufficient enough to discriminate ctDNA analogs in complex biological systems.

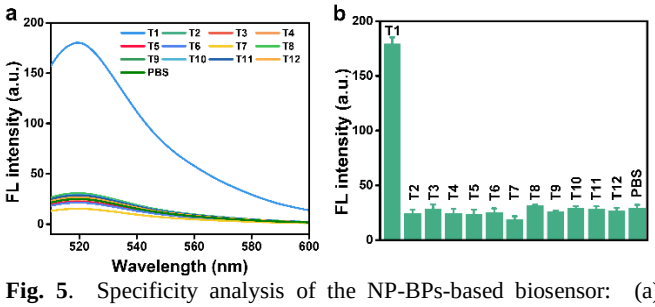

Fig. 5. Specificity analysis of the NP-BPs-based biosensor: (a) Fluorescence emission spectrum (excited by 488 nm) and (b) FL intensities of the NP-BPs-based biosensor in the presence of target ctDNA (T1), single-base mismatched ctDNA (T2, T3, T4, T6, T7, T8, T9), single-base deletion DNA (T5), short targets (T10, T11 and T12)

and Tris-HCl buffer. The error bars represent the standard deviation of three samples under same condition.

Conclusions

In this work, we have successfully fabricated a NP-BPs biosensor owing to its different affinities towards ssDNA and dsDNA. This NP-BPs biosensor has been fabricated by surface functionalization of BPs with nitrophenyl, which synergistically increases stability of BPs, enhances hydrophobic and π−π stacking interactions between the biosensor and nucleotide bases, and hence provides specific detection performances towards ctDNA. This biosensor shows a great advantage in ctDNA detection with an excellent sensitivity of 50 fM and a wide linear detection range of 50 fM-80 pM. In addition to robustness and specificity in single nucleotide polymorphisms discrimination, this NP-BPs biosensor demonstrate the accurate detection of ctDNA in the clinic serum samples. At the same time, the detection process is simple with good reproducibility and only takes 15 minutes. Although more ctDNA targets should be included in future experiments, this non-enzymatic biosensor holds clinical potentials in boasting rapid and accurate detection of ctDNA in cancer diagnosis, prognostic evaluation, and so on.

Acknowledgements

This work was supported by the National Natural Science Foundation of China (31971368, 51672305), Shenzhen Engineering Laboratory of Single-molecule Detection and Instrument Development (Grant No. XMHT20190204002), Science and Technology Service Network Initiative of Chinese Academy of Sciences (KFJ-STS-SCYD-102), Leading Talents of Guangdong Province Program (00201520), as well as Hong Kong Research Grants Council (RGC) General Research Funds (GRF) Nos. CityU 11301215 and 11205617.

Appendix A. Supporting material

(DNA sequences, TEM images and AFM images of BPs, Raman spectra, zeta potentials and dynamic light scattering of both BPs and NP-BPs, concentration optimization of NP-BPs, $MgCl_2$ and KCl, comparison of biosensor performance between NP-BPs and BPs) are available in the online version of this article in the attached file.

References

Burrell, R.A., McGranahan, N., Bartek, J., Swanton, C., 2013. Nature 501(7467), 338-345.
Cao, Y., Tian, X., Gu, J., Liu, B., Zhang, B., Song, S., Fan, F., Chen, Y., 2018. Angew Chem Int Ed Engl 57(17), 4543-4548.
Castellanos-Gomez, A., 2015. Black Phosphorus: Narrow Gap, Wide Applications. J Phys Chem Lett 6(21), 4280-4291.
Das, J., Ivanov, I., Montermini, L., Rak, J., Sargent, E.H., Kelley, S.O., 2015. Nat Chem 7(7), 569-575.
Fu, J., Wang, H., 2018. Cancer Lett 412, 283-288.
Garcia-Olmo, D.C., Dominguez, C., Garcia-Arranz, M., Anker, P., Stroun, M., Garcia-Verdugo, J.M., Garcia-Olmo, D., 2010. Cancer Res 70(2), 560-567.
Goedecker, S., Teter, M., Hutter, J., 1996. Phys Rev B Condens Matter 54(3), 1703-1710.
Grimme, S., Antony, J., Ehrlich, S., Krieg, H., 2010. J Chem Phys 132(15), 154104.
Guo, Z., Zhang, H., Lu, S., Wang, Z., Tang, S., Shao, J., Sun, Z., Xie, H., Wang, H., Yu, X.-F., Chu, P.K., 2015. Adv. Funct. Mater. 25(45), 6996-7002.
Gupta, V.K., Yola, M.L., Qureshi, M.S., Solak, A.O., Atar, N., Ustundag, Z., 2013. Sensor Actuat B-Chem 188, 1201-1211.
Hu, P., Zhang, S., Wu, T., Ni, D., Fan, W., Zhu, Y., Qian, R., Shi, J., 2018. Adv Mater 30(31), 1801690.
Hu, X., Wang, Y., Liu, H., Wang, J., Tan, Y., Wang, F., Yuan, Q., Tan, W., 2017. Chem Sci 8(1), 466-472.
Huang, C., Wang, J., Lv, X., Liu, L., Liang, L., Hu, W., Luo, C., Wang, F., Yuan, Q., 2018. Langmuir 34(23), 6777-6783.
Karakas, B., Bachman, K.E., Park, B.H., 2006. Br J Cancer 94(4), 455-459.
Karimi-Maleh, H., Tahernejad-Javazmi, F., Atar, N., Yola, M.L., Gupta, V.K., Ensafi, A.A., 2015. Ind. Eng. Chem. Res. 54(14), 3634-3639.
Kawano, O., Sasaki, H., Endo, K., Suzuki, E., Haneda, H., Yukiue, H., Kobayashi, Y., Yano, M., Fujii, Y., 2006. Lung Cancer 54(2), 209-215.
Murtaza, M., Dawson, S.J., Tsui, D.W., Gale, D., Forshew, T., Piskorz, A.M., Parkinson, C., Chin, S.F., Kingsbury, Z., Wong, A.S., Marass, F., Humphray, S., Hadfield, J., Bentley, D., Chin, T.M., Brenton, J.D., Caldas, C., Rosenfeld, N., 2013. Nature 497(7447), 108-112.
Newman, A.M., Bratman, S.V., To, J., Wynne, J.F., Eclov, N.C., Modlin, L.A., Liu, C.L., Neal, J.W., Wakelee, H.A., Merritt, R.E., Shrager, J.B., Loo, B.W., Jr., Alizadeh, A.A., Diehn, M., 2014. Nat Med 20(5), 548-554.
Perdew, J.P., Burke, K., Ernzerhof, M., 1996. Phys Rev Lett 77(18), 3865-3868.
Ryder, C.R., Wood, J.D., Wells, S.A., Yang, Y., Jariwala, D., Marks, T.J., Schatz, G.C., Hersam, M.C., 2016. Nat Chem 8(6), 597-602.
Schwarzenbach, H., Hoon, D.S., Pantel, K., 2011. Nat Rev Cancer 11(6), 426-437.
Shi, B., Shin, Y.K., Hassanali, A.A., Singer, S.J., 2015. J Phys Chem B 119(34), 11030-11040.
Shukla, S., Maclennan, G.T., Hartman, D.J., Fu, P., Resnick, M.I., Gupta, S., 2007. Int J Cancer 121(7), 1424-1432.
Taly, V., Pekin, D., Benhaim, L., Kotsopoulos, S.K., Le Corre, D., Li, X., Atochin, I., Link, D.R., Griffiths, A.D., Pallier, K., Blons, H., Bouche, O., Landi, B., Hutchison, J.B., Laurent-Puig, P., 2013. Clin Chem 59(12), 1722-1731.
Wang, Q., Wang, W., Lei, J., Xu, N., Gao, F., Ju, H., 2013. Anal Chem 85(24), 12182-12188.
William H. Press, S.A.T., William T. Vetterling, Brian P. Flannery, 2007. Cambridge University Press.
Yew, Y.T., Sofer, Z., Mayorga-Martinez, C.C., Pumera, M., 2017. Mater. Chem. Front., 1(6), 1130-1136.
Yola, M.L., Eren, T., Atar, N., 2014. Electrochimica Acta 125, 38-47.

Zhang, Y., Zheng, B., Zhu, C., Zhang, X., Tan, C., Li, H., Chen, B., Yang, J., Chen, J., Huang, Y., Wang, L., Zhang, H., 2015. Adv Mater 27(5), 935-939.
Zhou, J., Li, Z., Ying, M., Liu, M., Wang, X., Wang, X., Cao, L., Zhang, H., Xu, G., 2018. Nanoscale 10(11), 5060-5064.
Zhou, Q., Zheng, J., Qing, Z., Zheng, M., Yang, J., Yang, S., Ying, L., Yang, R., 2016.. Anal Chem 88(9), 4759-4765.
Zhou, W., Cui, H., Ying, L., Yu, X.F., 2018. Angew Chem Int Ed 57(32), 10268-10272.

Highlights

1. Two-dimensional biosensor has been fabricated to detect DNA in human serum samples.
2. NP-BPs biosensor shows high selectivity and excellent sensitivity towards ctDNA.
3. The proposed biosensing approach provide keys to accelerate the clinical potential boasting rapid, and accurate detection of ctDNA.

Declaration of interests

☒ The authors declare that they have no known competing financial interests or personal relationships that could have appeared to influence the work reported in this paper.

☐The authors declare the following financial interests/personal relationships which may be considered as potential competing interests: